LANGMUIR

Article

Temperature-dependent charge transport through individually contacted DNA origami-based Au nanowires

Bezu Teschome, Stefan Facsko, Tommy Schönherr, Jochen Kerbusch, Adrian Keller, and Artur Erbe

Langmuir, **Just Accepted Manuscript** • DOI: 10.1021/acs.langmuir.6b01961 • Publication Date (Web): 14 Sep 2016

ACS Publications

Langmuir is published by the American Chemical Society. 1155 Sixteenth Street N.W., Washington, DC 20036

Temperature-dependent charge transport through individually contacted DNA origami-based Au nanowires

Bezu Teschome[*,a,b,] *Stefan Facsko*[a], *Tommy Schönherr*[a], *Jochen Kerbusch*[a], *Adrian Keller*[c], *Artur Erbe*[*,a]

[a]Institute of Ion Beam Physics and Materials Research, Helmholtz-Zentrum Dresden-Rossendorf, 01328 Dresden, Germany.

[b]Technische Universität Dresden, Mommsenstraße 13, 01069 Dresden, Germany.

[c]Technical and Macromolecular Chemistry, University of Paderborn, Warburger Str. 100, 33098 Paderborn, Germany.

KEYWORDS. DNA origami, gold nanoparticles, metallization, electrical contacting, charge transport

ABSTRACT. DNA origami nanostructures have been used extensively as scaffolds for numerous applications such as for organizing both organic and inorganic nanomaterials, studying single molecule reactions and fabricating photonic devices. Yet, little has been done towards the integration of DNA origami nanostructures into nanoelectronic devices. Among other challenges,

the technical difficulties in producing well-defined electrical contacts between macroscopic electrodes and individual DNA origami-based nanodevices represents a serious bottleneck that hinders the thorough characterization of such devices. Therefore, in this work, we have developed a method to electrically contact individual DNA origami-based metallic nanowires using electron beam lithography. We then characterize the charge transport of such nanowires in the temperature range from room temperature down to 4.2 K. The room temperature charge transport measurements exhibit ohmic behavior, whereas at lower temperatures, multiple charge transport mechanisms such as tunneling and thermally assisted transport start to dominate. Our results confirm that charge transport along metallized DNA origami nanostructures may deviate from pure metallic behavior due to several factors including partial metallization, seed inhomogeneities, impurities, and weak electronic coupling among AuNPs. Besides, this study further elucidates the importance of variable temperature measurements for determining the dominant charge transport mechanisms for conductive nanostructures made by self-assembly approaches.

INTRODUCTION

One-dimensional (1D) nanostructures, such as nanotubes, nanorods and nanowires have received broad interest due to the unique properties associated with their nanoscale dimensions and their potential for integration with semiconductor devices.[1,2] Particularly, metallic nanowires have attracted a great deal of attention as they can be used as interconnects in fabricating nanoelectronic devices[3] and for chemical and biological sensing applications,[4] mainly due to their high surface-to-volume ratio and their fundamental electronic and optoelectronic properties as a result of quantum confinement effects.[5] In the past, various routes for the fabrication of 1D nanostructures have been demonstrated.[6,7] Among other methods, molecular self-assembly[7] has

shown great promise for the synthesis of both organic and inorganic nanostructures. Particularly, DNA-based self-assembly[8] is currently considered a powerful and versatile method for constructing nanostructures with varying degrees of complexity. For instance, the DNA origami technique[9] introduced by Rothemund in 2006 has proven its capabilities as a reliable method for synthesizing well-defined organic nanostructures by folding a long single-stranded DNA scaffold with the help of short synthetic staple strands. By this method, quasi 1D DNA nanostructures have been demonstrated[10], and these DNA origami nanostructures have been further used as scaffolds for the precise positioning of metallic nanoparticles[11–17] with few nanometer resolution and for the fabrication of linear and branched metallic nanowires.[18–21] With the development of the DNA origami technique[9] the fabrication of complex DNA-based metallic nanostructures became possible since it allows for the synthesis of DNA origami templates of arbitrary shape,[9,22–25] as well as a selective metallization by decoration of selected regions of the DNA origami surface with DNA-modified nanoparticle seeds via hybridization to protruding staple strands.[19,21] Hence, metallization of various DNA origami shapes has been demonstrated.[18–21,26–28]

Although the metallization of DNA origami has been extensively studied, there are only few reports so far that show electrical measurements of the charge transport through the metallized DNA origami nanostructures.[19,21] In part, this is due to the technical difficulties in producing well-defined electrical contacts between macroscopic electrodes and individual DNA origami-based nanowires. Previously, electrical contacting was achieved by random deposition of the metallized DNA origami from solution onto arrays of inter digital electrode arrays with small gaps. The smaller the gap between the electrodes, the higher the probability that a metallized

DNA origami nanostructure bridges the gap while having electrical contact to both electrodes. Hence, achieving selective electrical contacts and investigating the effect of the morphologies of the contacted nanostructures are challenging in such settings.

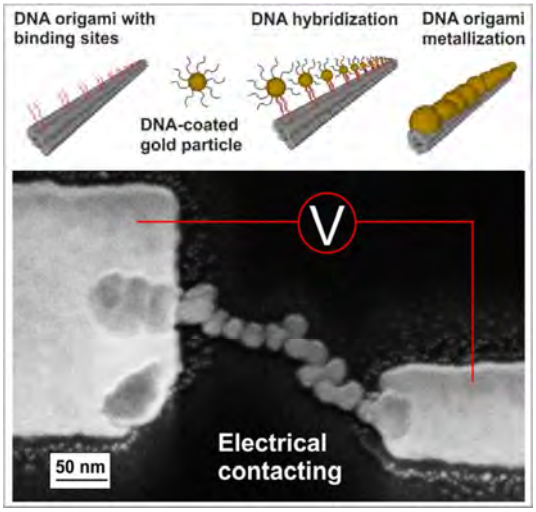

Figure 1. Schematic representation of the experimental approach for the synthesis, electrical contacting, and characterization of single DNA origami-templated metallic nanowires.

Therefore, in this work, we demonstrate the precise electrical contacting of individual metallized DNA origami nanowires and characterize their charge transport behavior at different bias voltages and temperatures. The schematic representation in figure 1 summarizes our experimental strategy. We first decorate DNA origami nanotubes with 14 AuNPs along the nanotube axis. Then, commercially available gold plating solution is applied to selectively grow the gold nanoparticles until they fuse with each other and create eventually continuous nanowires. Finally, we develop a method to electrically contact individual nanowires and characterize their charge transport behavior by I-V measurements at different temperatures.

Unlike the room temperature measurements which exhibit only ohmic behavior and agree with previously reported measurements,[19,21] the variable temperature measurements demonstrate the involvement of multiple charge transport mechanisms.

EXPERIMENTAL

The six-helix bundle DNA origami nanotube originally designed by Bui et al[10] was adopted as metallization template in this work. As previously reported,[29] the DNA origami assembly was performed by mixing the M13mp18 viral DNA scaffold (New England Biolabs) with the 170 staple strands (Metabion) in a 1:30 molar ratio in TAE buffer containing 20 mM Mg^{2+} (Sigma-Aldrich) in a total volume of 100 µL. For the attachment of AuNPs, 28 staple strands (Metabion) out of 170 total strands were modified on their 5' end with a protruding 5‘-$(AAT)_8T_4$-3‘ sequence, and citrate-stabilized 5 nm AuNPs (BBI) were coated with a complementary sequence 5‘-$(ATT)_3T_4$-3‘ as described previously.[11]

AuNP assembly on DNA origami nanotubes was performed at room temperature on 500 nm SiO_2 thermally grown on Si substrates. First, the SiO_2 substrate was cleaned in an oxygen plasma for 3 min and rinsed with ethanol and water. After drying the substrate in a stream of N_2, DNA origami solution (concentration ~1 nM) was deposited on the surface and incubated for 1 h in 10xTAE/200 mM Mg^{2+} in a humidity chamber. After incubation, the substrate was dipped in a 1:1 mixture of ethanol and Milli-Q water for 30 seconds to remove residual salt from the surface and dehydrate the DNA origami. After drying in a N_2 stream, hybridization of AuNPs with the immobilized DNA origami nanotubes was performed by depositing the DNA-coated AuNPs solution (concentration 50 nM) on the substrate surface and incubating further for 10 min at room temperature in 1 × TAE buffer containing 50 mM $MgCl_2$ as previously reported.[11] The

excess DNA-coated AuNPs and the residual salt were then removed by dipping the substrate first in Milli-Q water for 10 seconds and then in a 1:1 mixture of ethanol and Milli-Q water for 30 seconds. The concentration of the DNA-coated AuNPs solution was estimated by UV/vis spectroscopy from the optical absorbance at 520 nm. Imaging and characterization of AuNP modified DNA origami was performed by tapping mode atomic force microscopy (AFM) in air using a Bruker MultiMode 8 scanning probe microscope and PPP-NCLR cantilevers from Nanosensors (nominal force constant 48 N m–1, tip radius <10 nm).

For the metallization of AuNP modified DNA origami nanotubes, commercially available Au plating solution (GoldEnhance EM, Nanoprobes) was used. First, a 1:1 mixture of Au plating solution and 1x TAE buffer containing 10 mM Mg^{2+} was prepared. Then, the final solution was dropped immediately on the AuNP modified DNA origami surface and incubated for 10-20 min. The substrate was then dipped in Milli-Q water for 10 s and dried in a N_2 stream. Metallized DNA origami nanotubes were imaged by AFM and scanning electron microscopy (SEM). All the topographic AFM were analyzed using Gwyddion open source software.[30]

After the metallization process, the electrodes and the connection pads were fabricated using electron beam lithography (Raith eLINE Plus). First, ZEP (commercially available e-beam resist - Zeon) electron beam resist was spin coated on top of the substrate and baked at 150°C for 10 minutes. Then, the resist was exposed to an electron beam at 10 kV acceleration voltage. After electron exposure, the resist was developed by immersing the substrate first in N-amyl acetate for 90 seconds and then in isopropanol (IPA) for 30 seconds. A buffer layer of 5 nm Ti was then deposited on the sample by electron beam evaporation at a rate of 1 Å/s, followed by 50 nm Au

at a rate of 2.2 Å/s (working pressure ~ 10^{-9} mbar). After Au deposition, lift-off of resist was performed by submerging the substrate in acetone for 10 minutes and subsequent washing with IPA followed by drying in a stream of N_2.

All electrical measurements were carried out in vacuum (~ 10^{-5} mbar) in the dark using a Keithley 2400 source meter. For temperature dependent electrical characterization, a helium gas-flow cryostat system was used. To observe the effect of temperature on charge transport, samples were first cooled down to 4.2 K, and measurements were obtained when the samples were subsequently heated up to room temperature. All current measurements were obtained by sweeping the voltage range from -1V to +1V.

RESULTS AND DISCUSSION

For this work, quasi 1D DNA origami nanotubes with a nominal length of 412 nm and a nominal diameter of 6 nm were used. As previously reported,[11] the DNA origami nanotube was first modified to create 14 binding sites that can be used for the attachment of 14 AuNPs along the nanotube axis. Each binding site has two sticky ends protruding from two neighboring helices, and in total 28 staple strands were elongated by adding a capturing sequence on their 5' end (Figure 1). Figure 2a shows an AFM image with corresponding line scan (Figure 2a, inset) of the adsorbed and dried DNA origami nanotubes. The mean height of the nanotubes (Figure 2a, inset) is reduced by almost 3.5 nm due to dehydration and interaction with the surface.

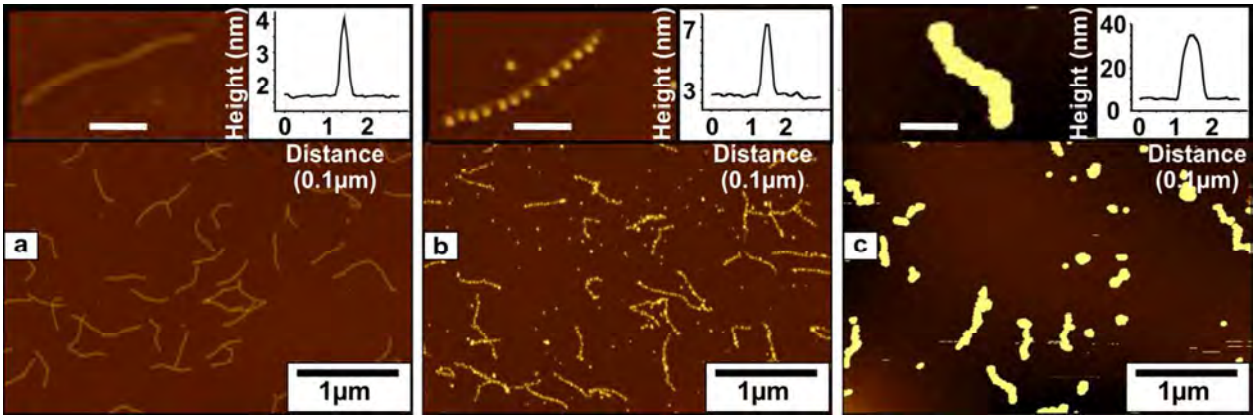

Figure 2. AFM height images with corresponding line scans (inset) for bare DNA origami nanotubes (a), AuNP-modified (b) and metallized (C) DNA origami nanotubes. All the topographic AFM images have 15 nm height scale. Insets have scale bars of 100 nm length.

For AuNPs attachment, we used our previously optimized protocol[11] to achieve a high nanoparticle assembly yield with few unbound background particles. Figure 2b shows an AFM image of AuNP-decorated DNA origami. An attachment yield > 96% was obtained, providing a high and uniform seed density which is essential for further metallization.

In order to optimize the metallization of the DNA origami nanotubes, various incubation times have been tested (see electronic supporting information). Figure 2c shows an AFM image of the metallized DNA origami nanotubes after 20 minutes of incubation time. The inset in figure 2c confirms that the 5 nm AuNP have grown to ~ 30 nm diameter. For better visualization, the sample was further characterized by SEM (Figure 3). The metallized DNA origami nanostructures are well-defined and appear continuous.

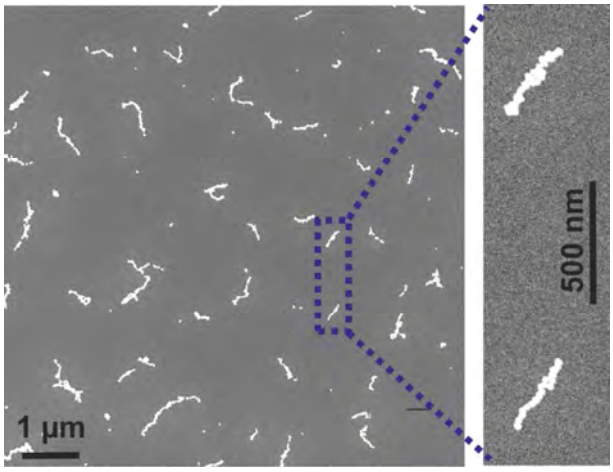

Figure 3. SEM image of metallized DNA origami nanotubes. The zoomed image shows the well-defined structure of the nanowires.

In order to electrically contact individual nanowires, we have developed an optimized method using electron beam lithography. First, parallel arrays of gold alignment marks (gap ~ 25 µm) were patterned using standard procedure on top of the SiO_2 substrate with pre-deposited DNA origami. Then, several SEM images were taken to determine a suitable nanowire density, corresponding to approximately one nanowire per 1 μm^2, and to register the x-y coordinates of the selected nanowires with respect to the alignment marks. After that, e-beam resist was deposited for defining contacts to selected nanowires. The registered location of the nanowires were then used to obtain the correct e-beam exposure position. In this way, electrical contacts to the individual nanowires were fabricated with high accuracy (Figure 4). Interestingly, the metallized DNA origami nanostructures strongly adhere to the substrate and sustain their shape during the lithography process. For the transport measurements, we contacted two nanowires with different morphologies. The first nanowire (NW-1, Figure 4a) consists of closely packed AuNPs, and due to random nanoparticle aggregation, the width of the nanowire seems greater than the actual single nanowire (between 30 and 75 nm). The second nanowire (NW-2, Figure

4b), on the other hand, features only the AuNPs attached to the single DNA origami nanotube and thus has a smaller effective width around 30 nm. The zoomed image in Figure 4b shows, however, that there may be small gaps (~ 1 to 3 nm) between neighboring AuNPs. A closer inspection of the grown AuNPs in the zoom shown in figure 4b reveals that some of the AuNPs preferentially grown in a lateral direction, leaving very small gaps between neighboring AuNPs. Although it is unclear at the moment why the AuNPs show this lateral growth, we speculate that it results from hindered diffusion of gold ions in the narrow gaps between the particles i.e. the ions' diffusion is becoming less and less efficient with increasing particle size. Note that under our experimental conditions, both increasing the Au plating time and repeating the plating process did not solve this issue but only led to stronger particle aggregation and larger nanowire widths.

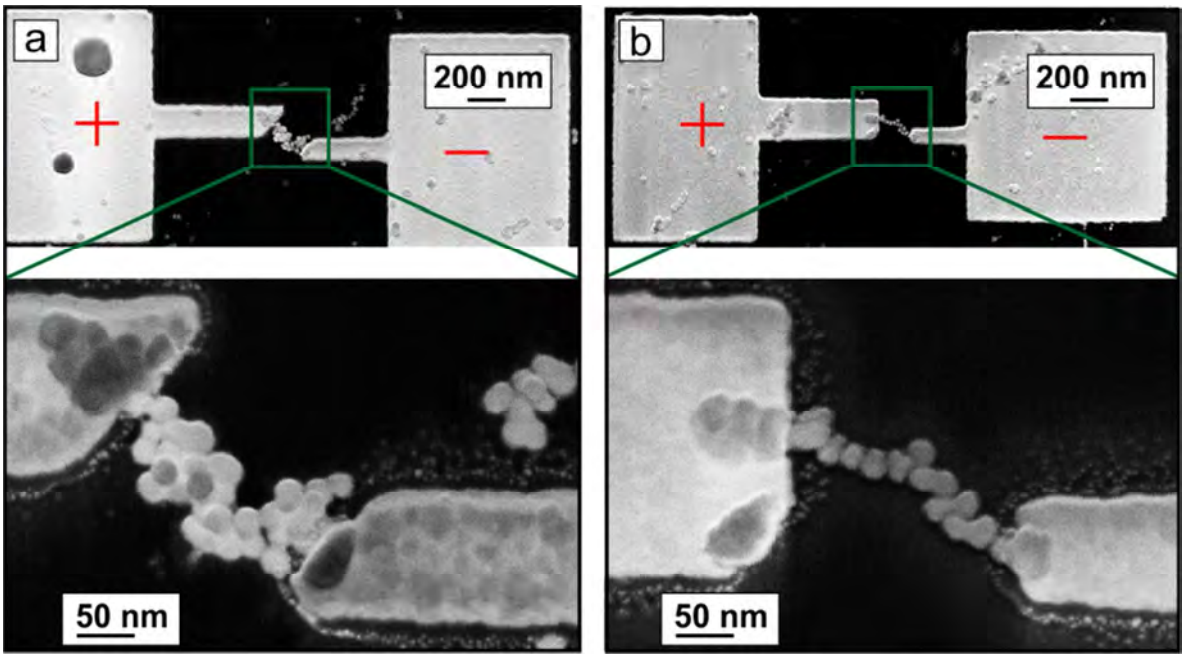

Figure 4. SEM images after electrical contacting of nanowire-1 (NW-1) (a) and nanowire-2 (NW-2) (b). The zoom images show the morphologies of both nanowires.

Two-terminal current-voltage measurements were performed on both nanowires in the temperature range between room temperature and 4.2 K and in the voltage range between – 1 V and + 1 V at ~ 10^{-5} mbar in the dark. The I-V curves in the insets of Figure 5a,b reveal that the two metallized nanowires exhibit ohmic behavior at room temperature with the measured current of NW-1 (Figure 5a, inset) being about 30 times larger than for NW-2 (Figure 5b, inset). This observation is consistent with the different morphologies of the nanowires as observed in Figure 4a,b and agrees with previously reported measurements[19,21] on metallized DNA origami nanostructures performed at room temperature. However, the measured resistance values of NW-1 (~ 116 MΩ) and NW-2 (~ 2.8 GΩ) are much higher than previously reported values of comparable nanowires (~ KΩ).[19] In addition, the variable-temperature measurements (4.2 K to 300 K) performed on both nanowires show that the electrical conductance of the nanowires decreases with temperature (Figure 5), contradicting purely metallic behavior.

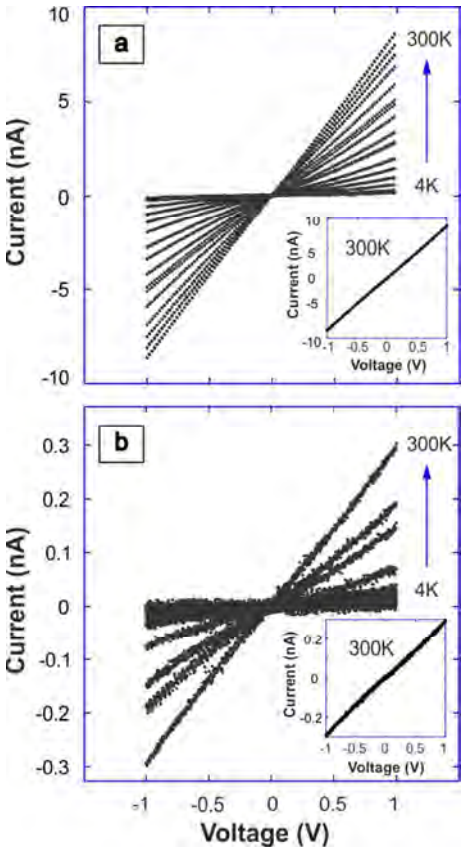

Figure 5. Temperature-dependent I-V characteristics for NW-1 (a) and NW-2 (b) over the temperature range from 4K to 300K. Insets are room-temperature I-V curves. All transport measurements were carried out under high vacuum in the dark.

To rationalize the electrical conductance of the nanowires, we consider several possible conduction mechanisms. Since the charge transport measurements show a decrease of conductance as a function of temperature, we first discuss temperature-dependent models such as hopping and thermionic emission conduction. In the hopping conduction model,[31–33] thermally activated electrons escape from one trap to another due to thermal fluctuations, and the conductance can be expressed in terms of temperature using,

$$G \sim \exp(-\frac{Ea}{kT}), \quad (1)$$

where G is the conductance, Ea the activation energy, k Boltzmann's constant and T the temperature. By plotting the natural logarithm of the conductance as a function of inverse temperature (ln(G) vs 1/T), we determine the thermally activated transport regime. Figure 6a displays the plot ln(G/G(300K) vs. 1/T for NW-1 and NW-2 at 1V positive bias voltage over the temperature range from 4.2 K to 300 K. Both nanowires show that at low temperatures, the conductance exhibits no significant temperature dependence, whereas at intermediate and high temperatures, thermally activated transport is observed. The respective activation energy[32] of each nanowire can be extracted from the slope of ln(G/G(300K) vs 1/T in figure 6b, which yields 24.1 meV for NW-1 and 72.5 meV for NW-2. The difference between the activation energy values of the two nanowires stems from their different morphologies and sizes. As seen in figure 4, NW-1 shows a much denser agglomeration of particles than NW-2. As a consequence, the

nanoparticles in NW-1 are forming a nanowire which has approximately twice the width of NW-2. This explains the lower energy of this wire compared to the thinner wire: The number of interconnects is increased by more than a factor of 2, and thus the transport energy is decreased by a similar factor. However, this linear fit holds only in the high temperature region from 100 K to 300 K for NW-1 and from 200 K to 300 K for NW-2, suggesting that hopping conduction dominates at higher temperatures.[32] We have also observed similar fits for different bias voltages which in turn supports the hopping conduction model. Hopping has been previously observed in metal contacts to self-assembled molecular monolayers with rather similar activation energies[34]. In such junctions, it could be shown that the activation energy depends on the nature and the surface morphology of the contacting metal[35]. Hence, the granularity of the metal leads to Coulomb blockade at low temperatures. In the DNA origami-based nanowires characterized in this work, however, the grain sizes are larger than in evaporated films; therefore Coulomb blockade effects are not observed. Besides, previous studies[36] on the conductivity along partially metallized λ-DNA also concluded that the transport at high temperature is dominated by hopping conduction. It is, however, presently unclear whether the thermally activated electrons hop along residual non-metallized DNA structures between grown AuNPs or through impurities.

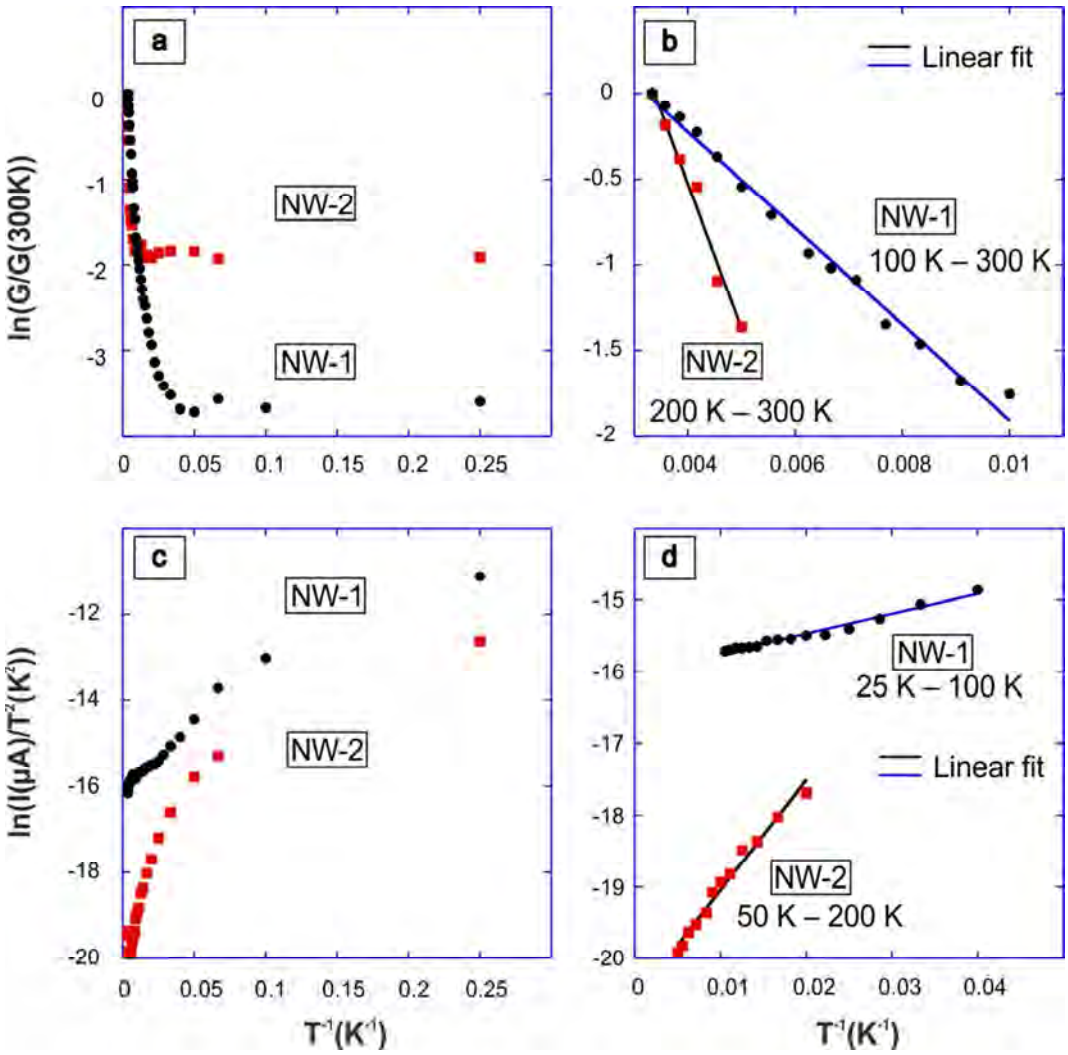

Figure 6. (a) Normalized natural logarithm of the conductance vs 1/T for NW-1 and NW-2 and (b) the respective linear fits to the data for certain temperature ranges. (c) Plots of ln (I/T2) vs 1/T for NW-1 and NW-2 and (d) the respective linear fits to the data points for certain temperature ranges. The fits in (b) and (d) reveal that thermally assisted transport is dominating in NW-1 at lower temperature than in NW-2.The voltage bias is 1V.

Similarly, the thermionic emission model in which electrons are thermally excited over the barrier instead of tunneling directly through the potential barrier is also examined. The temperature dependence of the current is given by,[37]

$$I \sim T^2 \exp\left(\frac{\phi - q\sqrt{qV/4\pi\varepsilon d}}{kT}\right) \qquad (2)$$

where, I is the current, T the temperature, ϕ the barrier height, V the bias, ε the dielectric constant, k Boltzmann's constant, d the barrier width, and q the electron charge. Figure 6c shows the plot of $\ln(I/T^2)$ vs 1/T for 1 V bias voltage for NW-1 and NW-2 over the temperature range from 4.2 K to 300 K. The linear fits in figure 6d demonstrate that similar to hopping conduction at high temperatures, thermionic emission is observed at lower temperatures between 25 K and 100 K for NW-1 and between 50 K and 200 K for NW-2. However, no thermally assisted transport is observed < 25 K for NW-1 and < 50 K for NW-2 (Figure 6a). Since the measured conductance at low temperature regimes is independent of temperature and follows a linear voltage dependence, the conduction mechanism can essentially be characterized by direct tunneling.[38] Although, direct tunneling is an important mechanism of transport in the self-assembled nanowires, it is difficult to extract the necessary parameters such as the barrier height from the tunneling current. It requires accurate measurements of the gap between the nanoparticles, which is not well-controlled under our experimental condition. Therefore, we conclude that different transport mechanisms are contributing to the overall transport in different temperature ranges. At low temperatures, the transport is dominated mainly by tunneling through the barrier, and as temperature increases the barrier decreases slightly, allowing more electrons to be excited over the barrier through a thermionic process. At high temperatures, hopping conduction governs the transport.

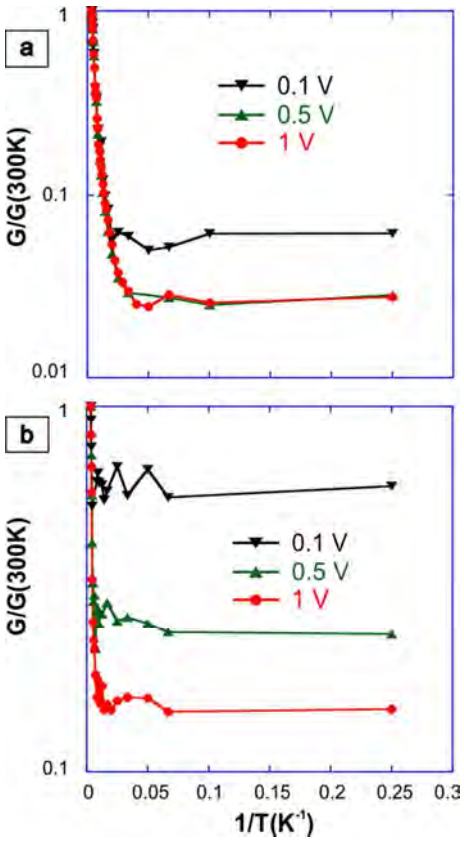

Figure 7. The natural logarithm of the normalized conductance vs 1/T for NW-1 (a) and NW-2 (b) for different biases.

We have also investigated the bias voltage dependence of the transport. Figure 7 depicts the conductance as a function of temperature for NW-1 (Figure 7a) and NW-2 (Figure 7b) at different forward bias voltages. In NW-2 (Figure 7b), no significant temperature dependence of the conductance is observed at low bias voltages (< 0.1 V), whereas in NW-1 (Figure 7a), thermally activated transport is found even at low bias voltages. We attribute this to the fact that the measured current at low bias voltage in NW-2 was too noisy to extract temperature dependent transport properly. Besides, at low bias voltage (0.1 V), a lower temperature dependency is observed in NW-2 compared to NW-1 (Figure 7), and as the voltage further increases (0.5 V), the effect of electric field becomes insignificant for NW-1. These observations

can again be explained by the different morphologies of the nanowires with NW-1 providing more paths than NW-2 for electrons to flow to the electrodes. Apart from this, the measured data exhibit no Fowler-Nordheim tunneling transport behavior. Therefore, we argue that the variable-temperature measurements not only elucidate the fact that the two nanowires reflect similar transport mechanisms despite their structural differences but also confirm that charge transport along metallized DNA origami nanostructures may deviate from pure metallic behavior due to several factors including partial metallization, seed inhomogeneities, impurities, and weak electronic coupling among AuNPs.

CONCLUSIONS

In summary, we have fabricated DNA origami-templated nanowires by metallization of DNA origami nanotubes and electrically contacted individual nanowires using electron beam lithography. We measured the electrical conductance of the metallized nanowires at various temperatures from room temperature down to liquid helium temperature for two different nanowire morphologies. At room-temperature, the I-V curves for both nanowires showed linear behavior, in agreement with previous reports. However, the temperature-dependent measurements indicate that multiple transport mechanisms contribute to the overall conductance of the nanowires in different temperature regimes. At low temperature, tunneling dominates the transport, whereas at intermediate and high temperatures, thermionic and hopping conduction governs the charge transport, respectively. Although the metallized DNA origami nanotubes deviate from pure metallic behavior, further tuning of the transport behavior is possible either by improving the metallization process or adding conductive molecules between the grown AuNPs which can be used for developing novel electronic devices displaying new functionalities.[39,40]

ASSOCIATED CONTENT

Supporting Information. Metallization of DNA origami nanotubes, other conduction mechanisms at lower temperatures. This material is available free of charge via the Internet at http://pubs.acs.org.

AUTHOR INFORMATION

Corresponding Authors

*b.teschome@hzdr.de

*a.erbe@hzdr.de

ACKNOWLEDGMENT

This work was kindly supported by the Initiative and Networking Fund of the Helmholtz Association of German Research Centers through the International Helmholtz Research School for Nanoelectronic Networks, IHRS NANONET (VH-KO-606). The authors thank C. Neisser for supporting the helium gas-flow cryostat measurements.

REFERENCES

(1) Hu, J.; Odom, T. W.; Lieber, C. M. Chemistry and Physics in One Dimension: Synthesis and Properties of Nanowires and Nanotubes. *Acc. Chem. Res.* **1999**, *32* (5), 435–445.

(2) Xia, Y.; Yang, P.; Sun, Y.; Wu, Y.; Mayers, B.; Gates, B.; Yin, Y.; Kim, F.; Yan, H. One-Dimensional Nanostructures: Synthesis, Characterization, and Applications. *Adv. Mater.* **2003**, *15* (5), 353–389.

(3) Kovtyukhova, N. I.; Mallouk, T. E. Nanowires as Building Blocks for Self-Assembling Logic and Memory Circuits. *Chem. – Eur. J.* **2002**, *8* (19), 4354–4363.

(4) Kenry; Lim, C. T. Synthesis, Optical Properties, and Chemical–biological Sensing Applications of One-Dimensional Inorganic Semiconductor Nanowires. *Prog. Mater. Sci.* **2013**, *58* (5), 705–748.

(5) Feng, S. Q.; Yu, D. P.; Zhang, H. Z.; Bai, Z. G.; Ding, Y. The Growth Mechanism of Silicon Nanowires and Their Quantum Confinement Effect. *J. Cryst. Growth* **2000**, *209* (2–3), 513–517.

(6) Kline, T. R.; Tian, M.; Wang, J.; Sen, A.; Chan, M. W. H.; Mallouk, T. E. Template-Grown Metal Nanowires. *Inorg. Chem.* **2006**, *45* (19), 7555–7565.

(7) Guo, Y.; Xu, L.; Liu, H.; Li, Y.; Che, C.-M.; Li, Y. Self-Assembly of Functional Molecules into 1D Crystalline Nanostructures. *Adv. Mater.* **2015**, *27* (6), 985–1013.
(8) Seeman, N. C. DNA in a Material World. *Nature* **2003**, *421* (6921), 427–431.
(9) Rothemund, P. W. K. Folding DNA to Create Nanoscale Shapes and Patterns. *Nature* **2006**, *440* (7082), 297–302.
(10) Bui, H.; Onodera, C.; Kidwell, C.; Tan, Y.; Graugnard, E.; Kuang, W.; Lee, J.; Knowlton, W. B.; Yurke, B.; Hughes, W. L. Programmable Periodicity of Quantum Dot Arrays with DNA Origami Nanotubes. *Nano Lett.* **2010**, *10* (9), 3367–3372.
(11) Teschome, B.; Facsko, S.; Gothelf, K. V.; Keller, A. Alignment of Gold Nanoparticle-Decorated DNA Origami Nanotubes: Substrate Prepatterning versus Molecular Combing. *Langmuir* **2015**, *31* (46), 12823–12829.
(12) Kuzyk, A.; Schreiber, R.; Fan, Z.; Pardatscher, G.; Roller, E.-M.; Högele, A.; Simmel, F. C.; Govorov, A. O.; Liedl, T. DNA-Based Self-Assembly of Chiral Plasmonic Nanostructures with Tailored Optical Response. *Nature* **2012**, *483* (7389), 311–314.
(13) Acuna, G. P.; Moller, F. M.; Holzmeister, P.; Beater, S.; Lalkens, B.; Tinnefeld, P. Fluorescence Enhancement at Docking Sites of DNA-Directed Self-Assembled Nanoantennas. *Science* **2012**, *338* (6106), 506–510.
(14) Takabayashi, S.; Klein, W. P.; Onodera, C.; Rapp, B.; Flores-Estrada, J.; Lindau, E.; Snowball, L.; Sam, J. T.; Padilla, J. E.; Lee, J.; et al. High Precision and High Yield Fabrication of Dense Nanoparticle Arrays onto DNA Origami at Statistically Independent Binding Sites. *Nanoscale* **2014**, *6* (22), 13928–13938.
(15) Schreiber, R.; Do, J.; Roller, E.-M.; Zhang, T.; Schüller, V. J.; Nickels, P. C.; Feldmann, J.; Liedl, T. Hierarchical Assembly of Metal Nanoparticles, Quantum Dots and Organic Dyes Using DNA Origami Scaffolds. *Nat. Nanotechnol.* **2014**, *9* (1), 74–78.
(16) Klein, W. P.; Schmidt, C. N.; Rapp, B.; Takabayashi, S.; Knowlton, W. B.; Lee, J.; Yurke, B.; Hughes, W. L.; Graugnard, E.; Kuang, W. Multiscaffold DNA Origami Nanoparticle Waveguides. *Nano Lett.* **2013**, *13* (8), 3850–3856.
(17) Gates, E. P.; Jensen, J. K.; Harb, J. N.; Woolley, A. T. Optimizing Gold Nanoparticle Seeding Density on DNA Origami. *RSC Adv* **2014**, *5* (11), 8134–8141.
(18) Schreiber, R.; Kempter, S.; Holler, S.; Schüller, V.; Schiffels, D.; Simmel, S. S.; Nickels, P. C.; Liedl, T. DNA Origami-Templated Growth of Arbitrarily Shaped Metal Nanoparticles. *Small* **2011**, *7* (13), 1795–1799.
(19) Pearson, A. C.; Liu, J.; Pound, E.; Uprety, B.; Woolley, A. T.; Davis, R. C.; Harb, J. N. DNA Origami Metallized Site Specifically to Form Electrically Conductive Nanowires. *J. Phys. Chem. B* **2012**, *116* (35), 10551–10560.
(20) Liu, J.; Geng, Y.; Pound, E.; Gyawali, S.; Ashton, J. R.; Hickey, J.; Woolley, A. T.; Harb, J. N. Metallization of Branched DNA Origami for Nanoelectronic Circuit Fabrication. *ACS Nano* **2011**, *5* (3), 2240–2247.
(21) Geng, Y.; Pearson, A. C.; Gates, E. P.; Uprety, B.; Davis, R. C.; Harb, J. N.; Woolley, A. T. Electrically Conductive Gold- and Copper-Metallized DNA Origami Nanostructures. *Langmuir* **2013**, 29 (10), 3482–3490.
(22) Andersen, E. S.; Dong, M.; Nielsen, M. M.; Jahn, K.; Subramani, R.; Mamdouh, W.; Golas, M. M.; Sander, B.; Stark, H.; Oliveira, C. L. P.; et al. Self-Assembly of a Nanoscale DNA Box with a Controllable Lid. *Nature* **2009**, *459* (7243), 73–76.
(23) Douglas, S. M.; Dietz, H.; Liedl, T.; Högberg, B.; Graf, F.; Shih, W. M. Self-Assembly of DNA into Nanoscale Three-Dimensional Shapes. *Nature* **2009**, *459* (7245), 414–418.

(24) Dietz, H.; Douglas, S. M.; Shih, W. M. Folding DNA into Twisted and Curved Nanoscale Shapes. *Science* **2009**, *325* (5941), 725–730.
(25) Han, D.; Pal, S.; Nangreave, J.; Deng, Z.; Liu, Y.; Yan, H. DNA Origami with Complex Curvatures in Three-Dimensional Space. *Science* **2011**, *332* (6027), 342–346.
(26) Pilo-Pais, M.; Goldberg, S.; Samano, E.; LaBean, T. H.; Finkelstein, G. Connecting the Nanodots: Programmable Nanofabrication of Fused Metal Shapes on DNA Templates. *Nano Lett.* **2011**, *11* (8), 3489–3492.
(27) Helmi, S.; Ziegler, C.; Kauert, D. J.; Seidel, R. Shape-Controlled Synthesis of Gold Nanostructures Using DNA Origami Molds. *Nano Lett.* **2014**, *14* (11), 6693–6698.
(28) Sun, W.; Boulais, E.; Hakobyan, Y.; Wang, W. L.; Guan, A.; Bathe, M.; Yin, P. Casting Inorganic Structures with DNA Molds. *Science* **2014**, *346* (6210), 1258361–1258361.
(29) Teshome, B.; Facsko, S.; Keller, A. Topography-Controlled Alignment of DNA Origami Nanotubes on Nanopatterned Surfaces. *Nanoscale* **2014**, *6* (3), 1790.
(30) Nečas, D.; Klapetek, P. Gwyddion: An Open-Source Software for SPM Data Analysis. *Open Phys.* **2012**, *10* (1).
(31) Morris, J. E.; Coutts, T. J. Electrical Conduction in Discontinuous Metal Films: A Discussion. *Thin Solid Films* **1977**, *47* (1), 3–65.
(32) Barwiński, B. Temperature Dependence of Electrical Conduction in Discontinuous Gold Films on Sapphire Substrates. *Thin Solid Films* **1985**, *128* (1), 1–9.
(33) Brust, M.; Bethell, D.; Kiely, C. J.; Schiffrin, D. J. Self-Assembled Gold Nanoparticle Thin Films with Nonmetallic Optical and Electronic Properties. Langmuir 1998, 14 (19), 5425–5429.
(34) Zhitenev, N. B.; Erbe, A.; Bao, Z. Single- and Multigrain Nanojunctions with a Self-Assembled Monolayer of Conjugated Molecules. Phys. Rev. Lett. 2004, 92 (18), 186805.
(35) Zhitenev, N. B.; Erbe, A.; Bao, Z.; Jiang, W.; Garfunkel, E. Molecular Nano-Junctions Formed with Different Metallic Electrodes. Nanotechnology 2005, 16 (4), 495.
(36) Kodama, T.; Jain, A.; Goodson, K. E. Heat Conduction through a DNA−Gold Composite. Nano Lett. 2009, 9 (5), 2005–2009.
(37) Wang, W.; Lee, T.; Reed, M. A. Mechanism of Electron Conduction in Self-Assembled Alkanethiol Monolayer Devices. Phys. Rev. B 2003, 68 (3), 35416.
(38) Wang, W.; Lee, T.; Reed, M. A. Mechanism of Electron Conduction in Self-Assembled Alkanethiol Monolayer Devices. Phys. Rev. B 2003, 68 (3), 35416.
(39) Sendler, T.; Luka-Guth, K.; Wieser, M.; Lokamani; Wolf, J.; Helm, M.; Gemming, S.; Kerbusch, J.; Scheer, E.; Huhn, T.; et al. Light-Induced Switching of Tunable Single-Molecule Junctions. *Adv. Sci.* **2015**, *2* (5), 1500017.
(40) Liao, J.; Blok, S.; Molen, S. J. van der; Diefenbach, S.; Holleitner, A. W.; Schönenberger, C.; Vladyka, A.; Calame, M. Ordered Nanoparticle Arrays Interconnected by Molecular Linkers: Electronic and Optoelectronic Properties. *Chem. Soc. Rev.* **2015**, *44* (4), 999–1014.

TOC graphic:

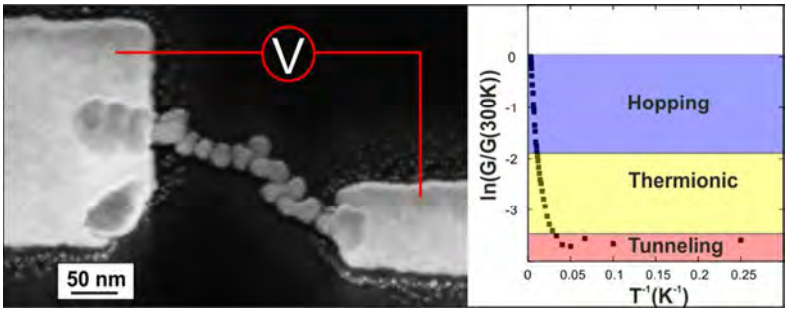
V
50 nm
ln(G/G(300K))
0
-1
-2
-3
Hopping
Thermionic
Tunneling
0
0.05
0.1
0.15
0.2
0.25
T-1(K-1)